Synthesis and Characterization of Perylenediimide Labeled Core−Shell Hybrid Silica−Polymer Nanoparticles

Tânia Ribeiro, Carlos Baleizão, and José Paulo S. Farinha*

Centro de Química-Física Molecular (CQFM) and Institute of Nanoscience and Nanotechnology (IN), Instituto Superior Técnico, 1049-001 Lisboa, Portugal

Received: July 16, 2009; Revised Manuscript Received: August 31, 2009

We have successfully synthesized core−shell nanoparticles with a silica fluorescent core and a methacrylate shell for application in photoactive high performance coatings and paints. Silica core particles with diameters between 270 and 440 nm and low polydispersity were labeled with a perylenediimide derivate with two terminal alkoxysilyl groups. Pure silica nanoparticles with equivalent diameters were also synthesized and surface modified with a second perylenediimide derivative. The photophysical properties of both sets of nanoparticles were studied for polarity environment dependence and dye aggregation. The fluorescent silica nanoparticles were surface modified with 3-(trimethoxysilyl)propyl methacrylate and used as seeds in the emulsion polymerization of a butyl or methyl methacrylate shell. Fluorescence correlation spectroscopy (FCS) was used to characterize the core−shell nanoparticles, using the fluorescent silica particles to calibrate the system. Films cast from water dispersions of clean core−shell nanoparticles are flexible, transparent, and exhibit fluorescence under appropriate excitation.

1. Introduction

Silica nanoparticles (SiNP) have been extensively used as supports or carriers in catalysis,[1] drug delivery,[2] imaging,[3] nanomedicine,[4] nanobiotechnology,[5] and bioanalysis.[6] Their characteristics can be tuned during the synthesis to obtain a wide range of particle diameters (20−500 nm) and different pore sizes, and to incorporate molecules such as catalysts, drugs, inorganic complexes, or fluorophores.[6] These molecules can be physically entrapped inside the core[6] or covalently attached to the silica network during the synthesis procedure, using the same strategy as for periodic mesoporous organosilicas.[7] Alternatively, the surface of SiNP can be functionalized postsynthesis with organic alkoxysilane compounds for covalent immobilization or adsorption of molecules and biomolecules[7] or to allow the synthesis of a polymer, metal, or inorganic shell.

From the different types of entities that can be incorporated in SiNP, photoactive molecules have emerged as one of the most interesting subjects, with applications in imaging,[3] bioanalysis,[6] optical sensors,[8] and photoactive materials.[9] The use of SiNP as fluorophore hosts has several advantages compared with polymer-based nanoparticles: there is usually less aggregation, the particles are more mechanically stable even at higher temperatures, and the increase in oxygen shielding enhances the dye photostability. This last point is an important issue for the continuous UV−vis irradiation of fluorophore doped SiNP, because the concentration of oxygen inside the SiNP is lower than in a regular solvent. For this reason, one expects the photostability of the fluorophore to be higher when incorporated in silica nanoparticles than for the free dye in solution or the dye anchored onto the SiNP surface.

In the past decade a new type of high performance coatings, based on hybrid organic/inorganic materials, has been developed, combining the polymer flexibility and ease of processing with the hardness of inorganic materials.[10] A general procedure to produce hybrid silica/polymer films is to incorporate the SiNP in a polymeric matrix which can give flexibility and transparency to the film, with the embedded SiNP conferring better mechanical properties.[11] For this purpose, the silica content of the final film must be optimized in order to simultaneously increase the tensile strength and impact resistance, without decreasing its flexural properties. A silica content of ca. 10 wt% is usually found to give the best film properties.[12] Incorporation of SiNP in polymer films is also known to reduce the thermal degradation of the film at high temperature, improve its insulation properties, and increase its barrier properties to solvents and volatile products generated during thermal decomposition of the film.[13] Polymers reinforced with surface-modified silica particles are particularly interesting because particle aggregation in the film is reduced, and therefore one expects composite coatings with even better scratch and abrasion resistance.[14] A methodology to obtain hybrid inorganic/polymeric films with a homogeneous distribution of the inorganic component and no aggregation in the film is to use hybrid core−shell (CS) nanoparticles with an inorganic core and a polymer shell.[11] The polymer shell is synthesized through a polymerization reaction after surface modification of the inorganic core. This true "a la carte" method can be used to obtain a wide range of materials due to the diversity of monomers that can be used to encapsulate the inorganic particles. To obtain hybrid films, a water dispersion of CS nanoparticles is cast onto a substrate and dried, allowing the particle shell to deform and occupy the voids between particles, yielding transparent and flexible films. Contrarily to films obtained by blending polymer and inorganic particles (for which transparency is mostly compromised),[15] this method can be used to obtain highly transparent nanohybrid materials. The mechanical properties of the hybrid films can be further improved by annealing at a temperature higher than the glass transition temperature (T_g) of the polymer shell, in order to allow interdiffusion of the polymer chains.

There are only a few examples in the literature of nanoparticles with a silica core and a polymer shell, using different

* Corresponding author: Telephone: +351 218419221. Fax: +351 218464455. E-mail: farinha@ist.utl.pt.

10.1021/jp906748r CCC: $40.75
Published on Web 09/25/2009

SCHEME 1: Silica Nanoparticles (SiNP) Labeled with Fluorescent Dye 2 on the Surface and Fluorescent Dye 1 Inside the Core; Encapsulation in a Polymer Shell

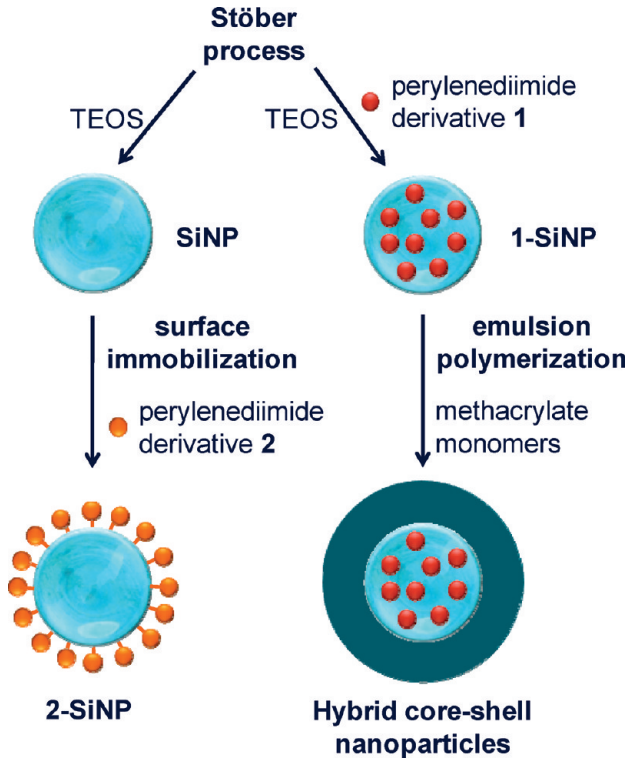

monomers and polymerization reactions: styrene (RAFT,[16] emulsion polymerization,[17] miniemulsion polymerization,[18] and dispersion polymerization[19]), *N*-isopropylacrylamide (RAFT,[20] emulsion polymerization,[21] redox-initiated graft polymerization[22]), methyl methacrylate (redox-initiated graft polymerization[22]), butyl acrylate (miniemulsion polymerization[18b] and dispersion polymerization[23]) and 2-hydroxypropyl methacrylate (dispersion polymerization[24]). As far as we know, there is no example of a CS hybrid nanoparticle doped in the silica core with a fluorescent molecule. This is a feasible challenge with an impact in several fields.

In the work presented here we have produced fluorescent core−shell hybrid nanoparticles, doped in the silica core with a perylenediimide derivative. The silica nanoparticles were obtained by the Stöber method using tetraethyl orthosilicate (TEOS) as a precursor. In one case a perylenediimide derivative having terminal triethoxysilyl groups was incorporated in the silica network during the particle synthesis. Other particles were surface modified with another perylenediimide dye (Scheme 1). The photophysics of the dyes was studied to evaluate the aggregation and the influence of the environment polarity in the dye. The silica nanoparticles encapsulating the dyes were modified with methacrylate groups and used as seeds in an emulsion polymerization procedure to produce a butyl or methyl methacrylate shell (Scheme 1). These hybrid silica−polymer core−shell nanoparticles were characterized by fluorescence correlation spectroscopy (FCS) and cast into films which are flexible, transparent, and fluorescent. The core−shell nanoparticles synthesized in this work provide a convenient and straightforward platform to generate fluorescent hybrid nanomaterials that can be used as high performance dyeing particles and coatings.

SCHEME 2: Structure of Perylenediimide Derivatives 1 and 2

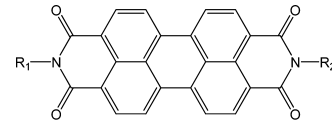

1: $R_1=R_2=CH_2CH_2CH_2Si(OEt)_3$
2: $R_1=CH_2CH_2CH_2CH_3$; $R_2=CH_2CH_2CH_2Si(OEt)_3$

2. Experimental Section

2.1. Materials. Absolute ethanol (Panreac, 99.5%), toluene spectroscopic (Aldrich, 99.9%), toluene anhydrous (Aldrich, 99.8%), ammonium hydroxide solution 25% (Fluka), tetraethyl orthosilicate (TEOS, Aldrich, 98%), 3-(trimethoxysilyl)propyl methacrylate (MPS, Aldrich, 98%), ethylene glycol dimethacrylate (EGDMA, Aldrich, 98%), sodium dodecyl sulfate (SDS, Sigma, 99%), and potassium persulfate (KPS, Aldrich, 99%) were used as received. Butyl methacrylate (BMA, Sigma-Aldrich, 99%) and methyl methacrylate (MMA, Aldrich, 99%) were distilled under vacuum prior to use. Deionized water from a Millipore system Milli-Q ≥18 MΩ cm was used in all synthesis steps. Perylenediimide derivatives **1** and **2** (Scheme 2) were synthesized according to the literature.[25,26] Pure silica nanoparticles and silica nanoparticles doped with **1** were synthesized by the Stöber method.[27]

2.2. Surface Modification of the Silica Nanoparticles with Compound 2. A solution of compound **2** (46 μL, 0.166 mmol/L) was added to a suspension of silica particles (300 mg) in dry toluene (10 mL), and allowed to reflux for 24 h under argon. After that time, the particles were centrifuged, decanted and repeatedly washed and decanted with chloroform, and finally dried in vacuum.

2.3. Surface Modification of the Silica Particles with Methacrylate Groups. The surface of the silica nanoparticles was modified with 3-(trimethoxysilyl)propyl methacrylate (MPS).[28] A suspension of silica nanoparticles in ethanol was stirred at 30 °C, and then MPS was added to the mixture (40 μmol of MPS/m^2 of SiO_2). The reaction proceeded for 48 h, and after that time the suspension was centrifuged (four cycles at 15 300 rpm of 15 min each). The MPS−silica nanoparticles were redispersed in absolute ethanol and dried at 60 °C.

2.4. Polymer Shell Synthesis. The polymer shell was prepared by seeded semicontinuous emulsion polymerization. Two sets of shells were prepared using methyl methacrylate or butyl methacrylate as monomer. In a typical procedure, a mixture of SDS and MPS-modified SiNP labeled with perylenediimide derivative **1** (MPS−**1**-SiNP) in water was purged with nitrogen for 30 min in a 100 mL three-necked glass reactor fitted with a condenser and a mechanical stirrer. The dispersion was then heated to 80 °C under argon. The distilled monomer and the cross-linking agent (syringe 1) and the KPS and SDS dissolved in the remaining water (syringe 2) were independently added to the reactor at a constant feed rate over 6 h. After the addition was complete, the reaction mixture was stirred for another 2 h. The dispersion of hybrid core−shell nanoparticles was adjusted to pH 7, diluted to 5 wt%, and cleaned with an ion-exchange resin (Bio-Rad AG 501-X8). The dispersion was stirred for 2 h and filtered afterward. CS1: 35.1 g of water, 1.0 g of MPS−**1**-SiNP1, 0.1 g of SDS, 4.6 g of butyl methacrylate, 0.1 g of KPS. CS2: 35.4 g of water, 1.0 g of MPS−**1**-SiNP4, 0.1 g of SDS, 3.4 g of butyl methacrylate, 0.1 g of KPS. CS3: 35.0 g of water, 1.0 g of MPS−**1**-SiNP3, 0.1 g of SDS, 4.9 g of methyl methacrylate, 0.1 g of KPS. CS4: 35.1 g of water,

1.0 g of MPS−**1**-SiNP3, 0.1 g of SDS, 4.8 g of methyl methacrylate, 0.21 g of ethylene glycol dimethacrylate, 0.1 g of KPS.

2.5. Characterization. The absorption spectra were recorded on a Shimadzu UV-3101PC UV−vis−NIR spectrophotometer, and the fluorescence measurements were obtained on a Spex Fluorolog F112A or in a SLM-Aminco 8110 Series 2 spectrofluorometer. The spectra of **1** and **2** were recorded in spectroscopic toluene in a quartz cell. The fluorescence quantum yield was determined using perylene in toluene as standard. The spectra of the nanoparticles in water dispersion were obtained in plastic cells with a I-shaped cross section in order to minimize the contamination of the spectra by light scattering. Films of silica nanoparticles were cast from the water dispersions onto glass slides. The glass slides were cleaned by dipping in a chromosulfuric acid solution for 1 h, washed with distilled water and dipped in an EDTA solution for 20 min, washed with distilled water again, and kept in distilled water, until they were dried with compressed air before use. Films of the core−shell hybrid nanoparticles were cast in a Teflon mold and dried at 30 °C in a ventilated oven.

Time-resolved picosecond fluorescence intensity decays were obtained by the single-photon timing method. The setup consists of a diode-pumped solid state Nd:YVO_4 laser (Milennia Xs, Spectra Physics) that can synchronously pump a mode-locked Ti:sapphire laser (Tsunami, Spectra Physics, with tuning range 700−1000 nm, output pulses of 100 fs, and 80 MHz repetition rate that can be reduced to 4 MHz by a pulse picker) or a cavity-dumped dye laser (701-2, Coherent, delivering 3−4 ps pulses of ca. 40 nJ $pulse^{-1}$ at 3.4 MHz) working with rhodamine 6G. Intensity decay measurements were made by alternating collection of impulse and decays with the emission polarizer set at the magic angle position. Impulses were recorded slightly away from the excitation wavelength with a scattering suspension. For the decays, a cutoff filter was used to effectively remove excitation light. Emission light was passed through a depolarizer before reaching the monochromator (Jobin-Yvon HR320 with a 100 lines/mm grating) and detected using a Hamamatsu 2809U-01 microchannel plate photomultiplier. No less than 10 000 counts were accumulated at the maximum channel. The decay curves were analyzed using a nonlinear least-squares reconvolution method.[29]

TEM images were obtained on a Hitachi transmission electron microscope (Model H-8100 with a LaB6 filament) with an accelerator voltage of 200 kV. The freeze-dried particles were dispersed in water or ethanol. One drop of dispersion was placed on a carbon grid and dried in air before observation.

Laser scanning confocal fluorescence microscopy (LSCFM) images were obtained with a Leica TCS SP5 laser scanning microscope using an HCX PL APO CS 1.20 W 63× water immersion objective (high magnification) and an HC PL APO CS 0.4 dry 10× (low magnification). Fluorescence correlation spectroscopy (FCS) curves were obtained with the same instrument, using an ISS VISTA correlator and software. The correlation curves were analyzed with the 3D-Gaussian ratio model.

3. Results and Discussion

3.1. Perylenediimide Derivatives. Perylenediimide dyes have very good properties for optical applications, including high fluorescence quantum yield, excitation in the visible region, small Stokes shift, and high photostability. Their preparation can be tailored to obtain symmetrical or asymmetrical compounds. Perylenediimide derivative **1** (Scheme 2) is symmetrical, with two propyltriethoxysilane groups that can be used to attach the dye to a silica network by two anchoring points, so that the dye becomes part of the network. It was obtained by condensation of perylene-3,4,9,10-tetracarboxylic dianhydride and 3-aminopropyltriethoxysilane.[25] The asymmetrical derivative **2** (Scheme 2) has only one propyltriethoxysilane group and therefore can be linked to a silica network by only one point. This avoids the co-condensation of the dyes (and consequent formation of aggregates with poor fluorescence properties) when one wants to label the surface of silica particles with relatively high dye content. It was prepared following a three-step route (hydrolysis of one anhydride moiety, condensation with butylamine, and a second condensation with 3-aminopropyltriethoxysilane).[26]

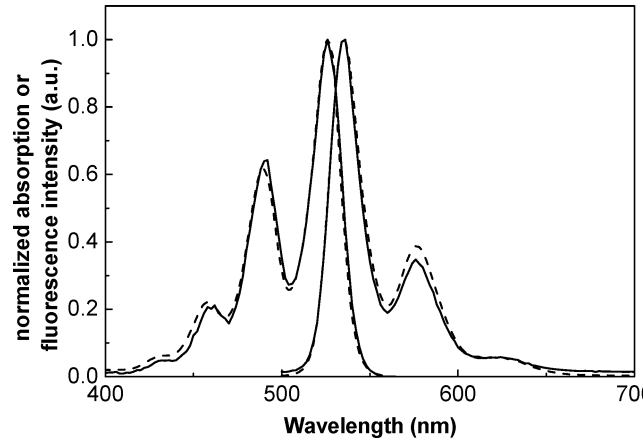

Figure 1. Normalized absorption and fluorescence spectra of perylenediimide derivatives **1** (solid curve) and **2** (dashed curve) in toluene.

The absorption and fluorescence spectra of perylenediimide derivatives **1** and **2** in toluene are shown in Figure 1. The two compounds exhibit the same intensity maxima, with absorption between 400 and 500 nm and fluorescence emission between 500 and 650 nm. The fluorescence quantum yields of both compounds dissolved in toluene are very high (0.83 ± 0.03 and 0.84 ± 0.02 for compounds **1** and **2**, respectively), and the fluorescence decay curves have single-exponential behavior, with lifetimes of 4.0 ns for derivative **1** and 4.1 ns for derivative **2**. These results indicate that the photophysical properties of the perylenediimide dyes **1** and **2** do not depend on the symmetry of the molecule and the amount of propyltriethoxysilane groups.

3.2. Synthesis of the Silica Nanoparticles. The silica nanoparticles (SiNP) were prepared following the Stobër method, using TEOS as the silica precursor.[27] Perylenediimide derivative **1** was also used as a secondary silica source to obtain fluorescent silica nanoparticles (**1**-SiNP), taking advantage of the two terminal triethoxysilyl groups. The dyes become part of the silica network, with the double attaching points severely restricting their movement and contributing to reduced fluorescence quenching. The fluorescent nanoparticles were characterized by transmission electron microscopy (TEM) and laser scanning confocal fluorescence microscopy (LSCFM). The images obtained by TEM and confocal microscopy were binarized and analyzed to measure the statistical nanoparticle diameter in order to obtain the size distribution histograms (Figure 2). Table 1 shows the statistical diameter of the nanoparticles obtained from several TEM and confocal microscopy images.

We prepared nanoparticles with diameters from ca. 270 to 440 nm with low polydispersity. This diameter range allows us to observe the particles by fluorescence confocal microscopy.

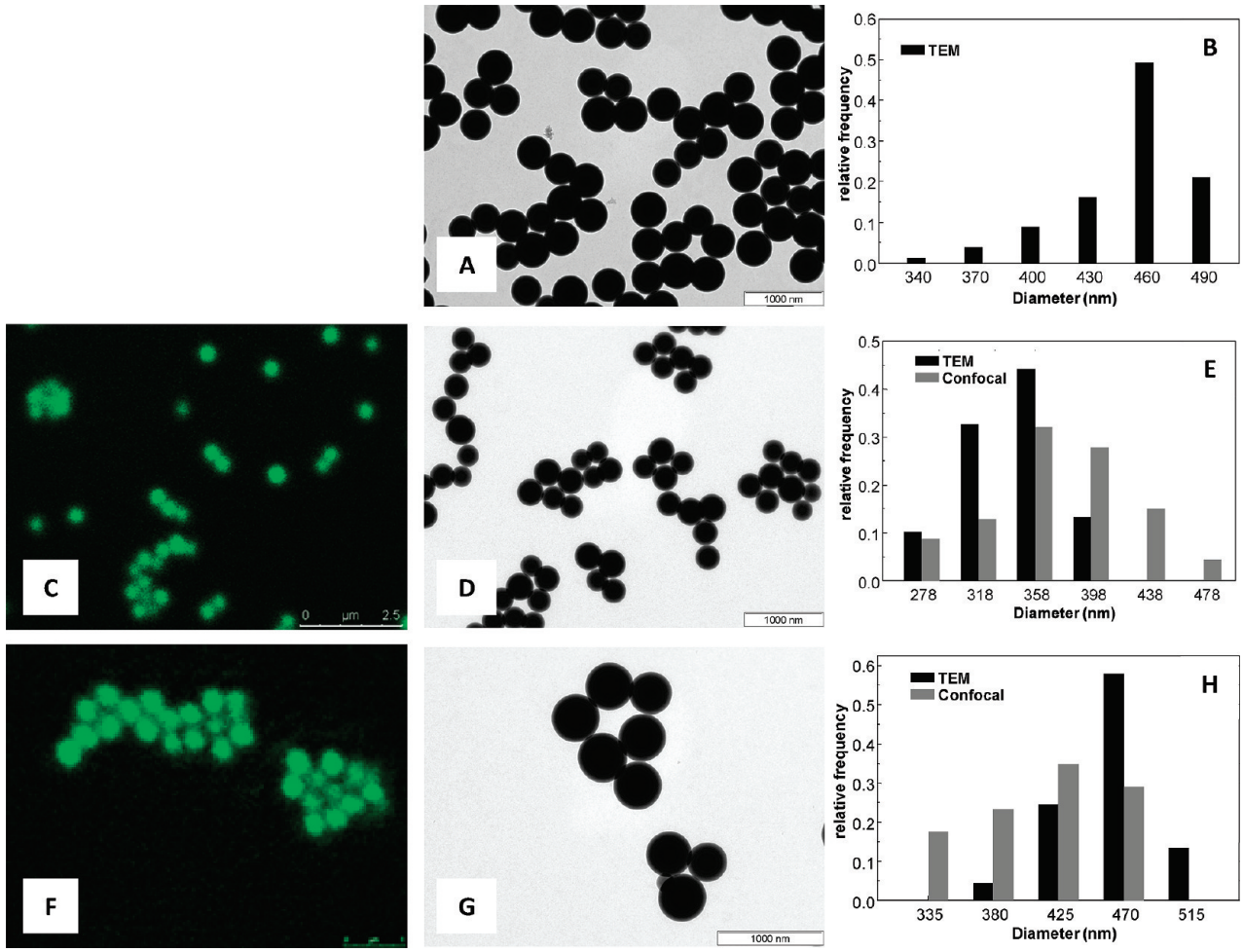

Figure 2. TEM images (A, D, and G, scale bar 1 μm), confocal fluorescence microscopy images (C, image size 10 μm × 10 μm; and F, image size 6.5 μm × 6.5 μm) and diameter distributions obtained for several images (B, E, and H) for SiNP2 (A and B), **1**-SiNP4 (C−E), and **1**-SiNP7 (F−H).

TABLE 1: Average Diameters Obtained from TEM and Fluorescence Confocal Microscopy for the Silica Nanoparticles

	diameter (nm)	
	TEM	confocal
SiNP1	320 ± 30	
SiNP2	440 ± 30	
1-SiNP3	270 ± 20	320 ± 40
1-SiNP4	320 ± 30	350 ± 50
1-SiNP5	400 ± 30	450 ± 60
1-SiNP6	410 ± 40	430 ± 60
1-SiNP7	440 ± 30	400 ± 50

The statistical diameters obtained by confocal microscopy are very similar to the values obtained by TEM, although the standard deviation of the diameters measured from the TEM images is smaller due to the increased contribution of experimental error in the LSCFM measurements.

The surface of the pure silica nanoparticles SiNP1 was modified with perylenediimine derivative **2**. This asymmetric derivative comprises a terminal propyltriethoxysilyl group, which can be immobilized on the surface of silica materials. Dye **2** has only one anchoring point to avoid dye aggregation during the labeling reaction. The **2**-SiNP1 particles were prepared by the condensation of SiNP1 with **2** in toluene. The photophysical characterization of both sets of perylenediimide labeled particles will be presented and discussed in the following sections.

3.3. Fluorescence of Labeled Silica Nanoparticles. We first show the influence of the surrounding media on the fluorescence of the labeled silica nanoparticles, and then we characterize the aggregation of the perylenediimide derivatives **1** and **2** when incorporated in the silica nanoparticles. In Figure 3 we show the fluorescence spectra of **1**-SiNP and **2**-SiNP1 in film and dispersed in water and in 1,4-dioxane, compared to the spectra of **1** and **2** in toluene.

The analysis of the fluorescence spectra from Figure 3 leads to interesting observations. The emission maximum of **1**-SiNP in the film and when dispersed in water suffers a shift to higher wavelengths when compared with the emission maximum of **1** in toluene and **1**-SiNP dispersed in 1,4-dioxane (Figure 3A). These results show that the solvent diffuses inside the nanoparticle, affecting the emission maximum of the dye according to the solvent polarity, which is a clear indication that the silica nanoparticles are porous. In water, the emission maximum of **1** suffers a solvatochromic shift to higher wavelengths, due to a higher stabilization of the S_1 excited state compared to the S_0 ground state in polar solvents. The decrease in energy observed in polar solvents means that the dipolar moment of **1** is higher in the excited state. When the particles are dispersed in 1,4-dioxane, the S_0 state is more stabilized than the S_1 state, increasing the energy difference between the two states. This way, we observed a shift to lower wavelengths of the nanoparticle emission in 1,4-dioxane, compared to the emission in water. The spectra of the particle dispersions in 1,4-dioxane

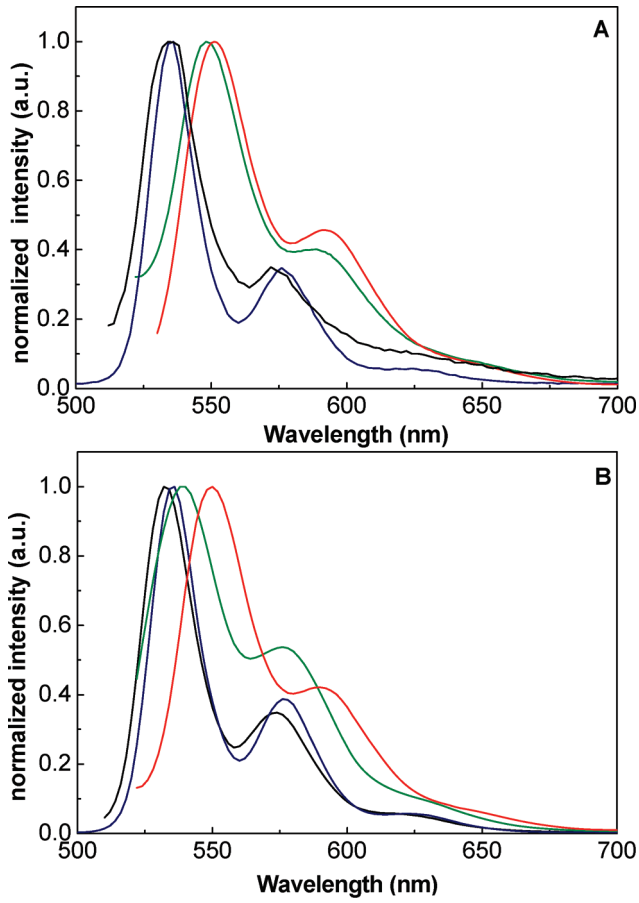

Figure 3. Normalized emission spectra of dye **1** in toluene (λ_{exc} = 490 nm, blue curve), and of the labeled particles **1**-SiNP in film (λ_{exc} = 495 nm, green curve), dispersed in water (λ_{exc} = 500 nm, red curve), and dispersed in 1,4-dioxane (λ_{exc} = 490 nm, black curve) (A). Normalized emission spectra of dye **2** in toluene (λ_{exc} = 460 nm, blue curve), and of the labeled particles **2**-SiNP in film (λ_{exc} = 470 nm, green curve), dispersed in water (λ_{exc} = 470 nm, red curve), and dispersed in 1,4-dioxane (λ_{exc} = 460 nm, black curve) (B). In both cases a solvatochromic shift of ca. 18 nm is observed between the spectra of the dyes in toluene and that of the labeled particles in water.

are similar to the spectra of **1** in toluene because the solvents have equivalent polarity. In the case of **1**-SiNP films, since the dye is incorporated inside the particles, and therefore surrounded by a polar medium (Si−O−Si bonds), the solvatochromic shift is similar to the one observed for **1**-SiNP dispersed in water.

For **2**-SiNP1 and perylenediimide **2** (Figure 3B), the emission maxima of the free dye in toluene and the particles dispersed in water and in 1,4-dioxane are similar to those obtained for **1**-SiNP and **1**. However, for **2**-SiNP1 films the emission maximum is similar to the maxima obtained for the particles dispersed in 1,4-dioxane and for dye **2** in toluene. This is because derivative **2** is located on the surface of the nanoparticles and in the powderlike films the silica nanoparticles do not deform, limiting the contact of the surface bound perylenediimide molecules with the silica environment.

An important problem with the use of perylenediimide derivatives in industrial applications is their tendency to aggregate, forming dimers or aggregates with less desirable spectroscopic properties.[30] The formation of these species can be studied by absorption or excitation measurements. The difference between the two types of experiments is that, while absorption detects both emissive and nonemissive aggregates, in excitation spectra we only observe the emissive species. In the present work, the absorption measurements were nonconclusive because scattering from the silica nanoparticles masked dye fluorescence. In any case, the presence of nonemissive aggregates would only decrease the fluorescence quantum yield of the dyes in the nanoparticles, an effect of no consequence for most applications.

To study the possible formation of emissive dye aggregates in our particles, we analyze the changes in the excitation spectra of **1**-SiNP obtained at different wavelengths. From the excitation spectra of **1** in toluene measured at different wavelengths, λ_{emi} = 535, 575, and 624 nm (Figure 4A), we calculate the intensity ratios I_{535}/I_{575} and I_{535}/I_{624} (Figure 4B,C). These ratios reveal no significant fluctuations, indicating that the same species are absorbing and emitting at the different wavelengths, and therefore there is no aggregate formation for **1** in toluene. For **2** in toluene there is also no aggregation as shown by the constant ratio of excitation spectra at different emission wavelengths (Figure 4D−F).

The same experiment was performed in water dispersions of **1**-SiNP6, recording the excitation spectra at emission wavelengths λ_{emi} = 545, 575, and 635 nm (Figure 5), and calculating the ratios I_{545}/I_{575} and I_{545}/I_{635} (Figure 5B,C). The fluctuations observed in the intensity ratios indicate the presence of ground state aggregates of **1** in the particles.[30] To evaluate the extent of aggregation, we compared the fluorescence excitation and emission spectra obtained for **1** in toluene and for **1**-SiNP6 dispersed in water (Figure 6A). The spectra are similar, apart from the solvatochromic shift observed in the **1**-SiNP discussed before. After correcting for this deviation, the difference between the two emission spectra reveals the presence of a new fluorescent species that probably corresponds to aggregates of **1** present in the labeled particles (Figure 6B).

For **2**-SiNP1 in water (Figure 7), the ratios I_{550}/I_{590} and I_{550}/I_{650} showed small fluctuations that suggested the presence of aggregates in the ground state. The emission and excitation spectra of **2** are similar to those of **2**-SiNP1 dispersed in water, although a red shift in the nanoparticle spectrum is also observed (Figure 8A). Correcting the shift and subtracting the spectra, we obtain an emission band that is attributed to the presence of emissive aggregates of **2** in the nanoparticles (Figure 8B).

These results reveal the presence of emissive dye aggregates both in particles labeled inside and at the surface, but the small extent of distortion in the spectra indicates that the degree of aggregation of **1** and **2** in the SiNP is fairly small when compared to other perylene derivatives immobilized in solid materials.[30] The perylenediimide dyes used here were designed to minimize aggregation either inside the particle or at the surface. Derivative **1** has two anchoring points to the silica network and thus becomes homogeneously distributed and immobile inside the particles; however it easily originates multiagregates by co-condensation if used to label the particle surface. On the other hand, dye **2** has only one anchoring point so that, once it binds to the silica surface, it cannot further react with another dye **2** molecule.

One important difference between the particles with the dyes inside and the particles labeled at the surface is the photostability of the dyes. Although perylene dyes are generally quite photostable, continuous irradiation of films of **1**-SiNP and **2**-SiNP1 on glass substrates at λ_{exc} = 495 nm using a 450 W Xe lamp shows that in a period of 10 h the fluorescence intensity of the surface labeled particles drops almost 14%, while no change is detected for the particles with the dyes inside (Figure 9). This is due to the oxygen barrier properties of the silica

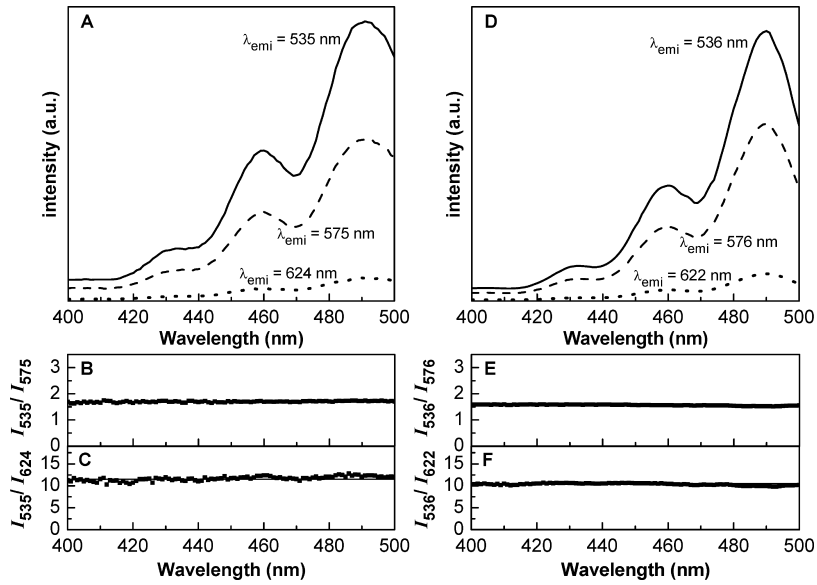

Figure 4. Excitation spectra of dyes **1** (A) and **2** (D) in toluene at different emission wavelengths. The intensity ratios I_{535}/I_{575} (B) and I_{535}/I_{624} (C) for **1** and I_{536}/I_{576} (E) and I_{536}/I_{622} (F) for **2**, show no significant fluctuations, indicating that there is no aggregate formation for **1** and **2** in toluene.

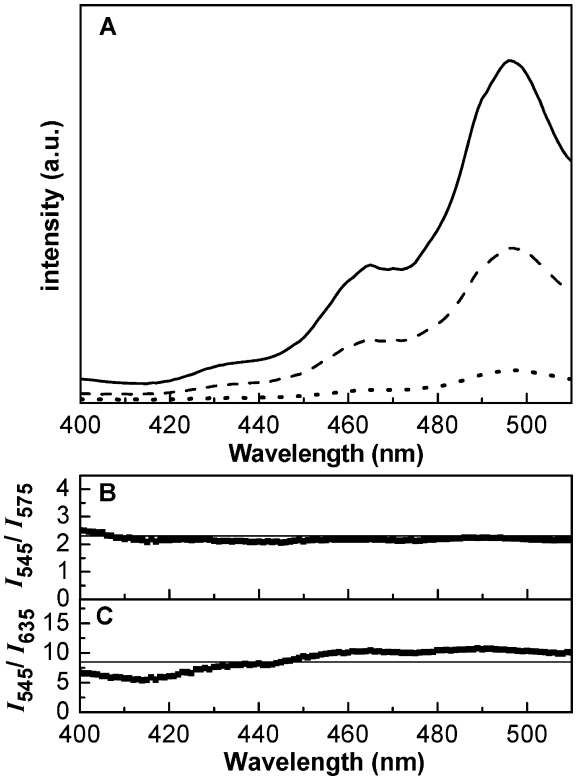

Figure 5. Excitation spectra of **1**-SiNP6 dispersed in water obtained at λ_{emi} = 545 (solid curve), 575 (dashed curve), and 635 nm (dotted curve) (A). The fluctuations observed in the intensity ratios I_{545}/I_{575} (B) and I_{545}/I_{635} (C) indicate the presence of ground state aggregates of **1** in the particles.

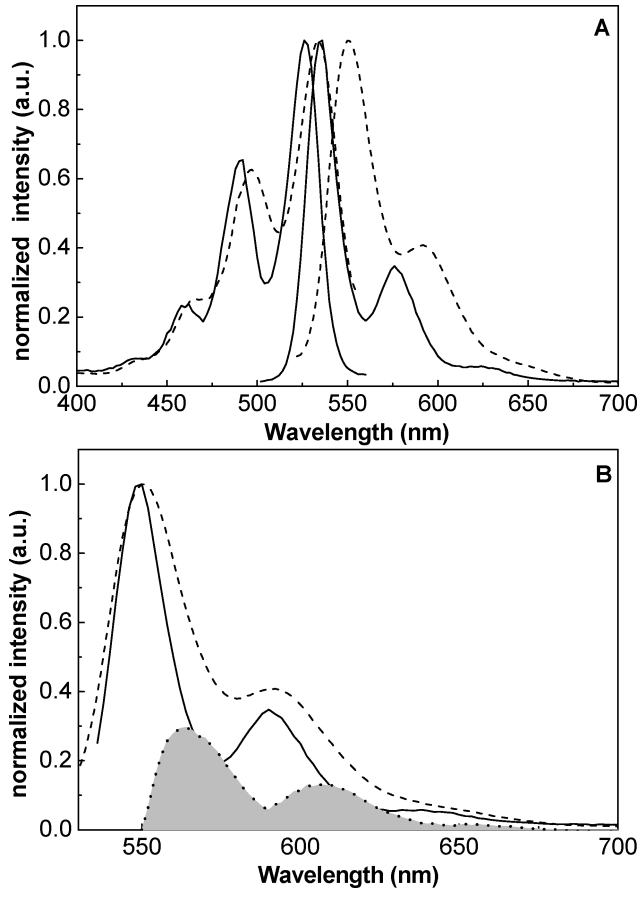

Figure 6. Normalized excitation (λ_{emi} = 575 nm) and emission spectra of **1** in toluene (λ_{exc} = 490 nm, solid curve) and **1**-SiNP6 in water (λ_{exc} = 495 nm, dashed curve) (A). Normalized and corrected emission spectra of **1** in toluene (solid curve) and **1**-SiNP6 in water (dashed curve) (B). The difference between the curves (B, filled dotted curve) reveal the presence of emissive aggregates of **1** in the labeled particles.

matrix, which effectively protects the dyes incorporated in the silica network.

3.4. Core−Shell Nanoparticles. The surface of the silica nanoparticles labeled with perylenediimide derivative **1** inside was surface modified with 3-(trimethoxysilyl)propyl methacrylate (MPS) to provide grafting sites for the synthesis of a polymer shell. The surface modification was carried out in ethanol under mild experimental conditions. The shell was synthesized by seeded semicontinuous emulsion polymerization, using SDS as surfactant, KPS as initiator, and butyl methacrylate or methyl methacrylate as monomers. In the case of methyl methacrylate, ethylene glycol dimethacrylate was used as cross-

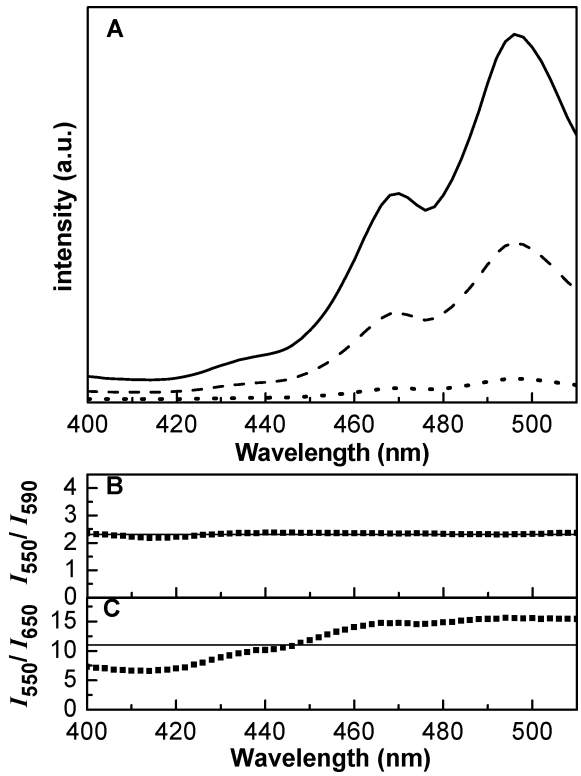

Figure 7. Excitation spectra of **2**-SiNP1 dispersed in water obtained at $\lambda_{emi} = 550$ (solid curve), 590 (dashed curve), and 650 nm (dotted curve) (A). The fluctuations observed in the intensity ratios I_{550}/I_{590} (B) and I_{550}/I_{650} (C) indicate the presence of ground state aggregates of **2** in the particles.

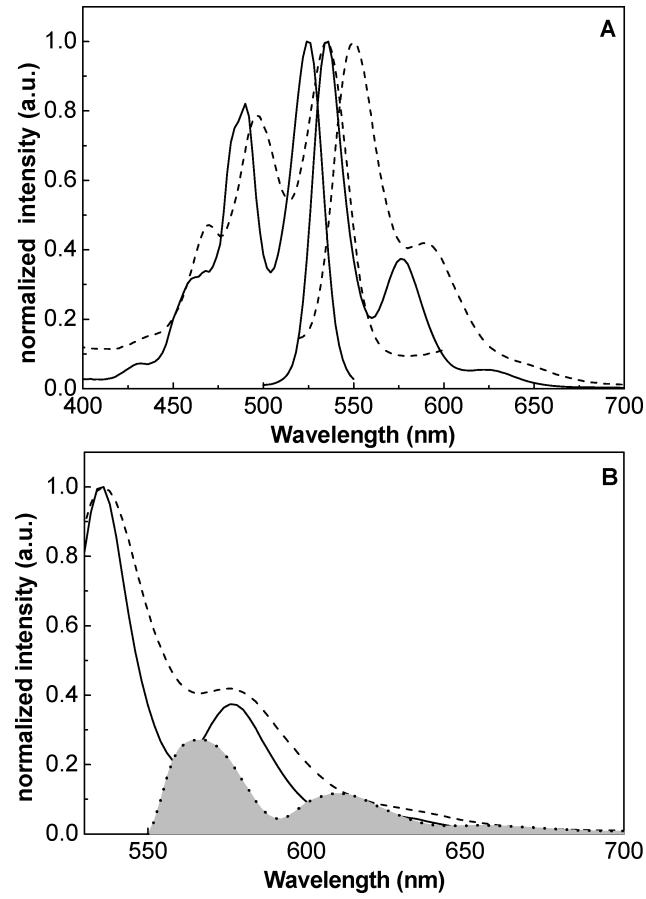

Figure 8. Normalized excitation and emission spectra of **2** in toluene ($\lambda_{emi} = 622$ nm and $\lambda_{exc} = 460$ nm, solid curve) and **2**-SiNP1 in water ($\lambda_{emi} = 650$ nm and $\lambda_{exc} = 470$ nm, dashed curve) (A). Normalized and corrected emission spectra of **2** in toluene (solid curve) and **2**-SiNP1 in water (dashed curve). The difference between the curves (B, filled dotted curve) reveals the presence of emissive aggregates of **2** in the labeled particles.

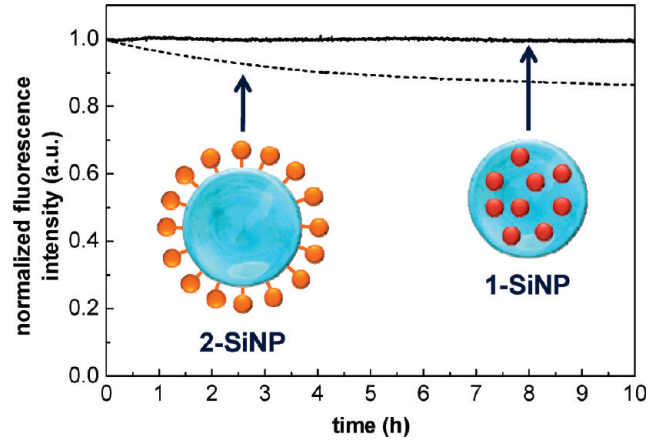

Figure 9. Fluorescence intensity of films of **1**-SiNP (solid curve) and **2**-SiNP1 (dashed curve) deposited on glass substrates and irradiated at $\lambda_{exc} = 495$ nm using a 450 W Xe lamp.

linking agent. In Table 2 we compile the characteristics of the core−shell nanoparticles (CS). In all cases we were able to obtain fairly monodispersed hybrid core−shell nanoparticles with 100% conversion (calculated from weight balance).

Our attempts to characterize the core−shell nanoparticles by TEM, dynamic light scattering (DLS), and static light scattering (SLS) were not conclusive. We were not able to determine the final diameter of the core−shell nanoparticles due to fluidification of the polymer shell under the TEM beam; $T_g \approx 30$ °C for poly(butyl methacrylate) (PBMA). As for DLS, we measured complex scattering curves with angle-dependent components from the core−shell particles, mixed with a weak signal from small particles (presumably resulting from a small amount of polymer nucleated out of the silica particles) and dust coming from the synthesis. In the SLS experiments, we could only detect the polymer shell encapsulating the solvent isorefractive silica core. To overcome this problem, we used fluorescence correlation spectroscopy (FCS) to measure the core−shell diameter of the particles with a perylenediimide labeled core. In this case, we only detected the diffusion of the labeled particles, with no interference from dust or (unlabeled) polymer material remaining in the dispersion, and with no constrains from scattering by large particles with a complex geometry. In order to evaluate the performance of the FCS technique for characterizing large particles, we started by measuring the silica particles **2**-SiNP1, using **1**-SiNP4 to calibrate the system. From the TEM average diameter (R_{TEM}) of **1**-SiNP4, we calculated the gyration radius of the particles $R_g = (3/5)^{0.5}R_{TEM}$, and since for hard spheres[31] $R_H = R_g/0.775$, from R_H we determined the particle diffusion coefficient using the Stokes−Einstein equation. This diffusion coefficient was fixed in order to obtain the calibration parameter for the system (w_0) from the FCS correlation curve of **1**-SiNP4 in water (Supporting Information). The w_0 value determined from the silica core was then used to analyze the correlation curve of **2**-SiNP1, from which we determined the diffusion coefficient ($D = 1.368$ $\mu m^2/s$) and calculated the respective hydrodynamic diameter ($D_H = 319$ nm). The diffusion coefficient is obtained by global fitting of several autocorrelation curves (Supporting Information). For long correlation times, the autocorrelation functions show some oscillation related to

TABLE 2: Composition, Hydrodynamic Diameters Determined by FCS, and Expected Diameters from the Mass Balances for the Core−Shell Nanoparticles

core−shell synthesis	core	monomer	cross-linking	D_H (nm)	D_{calc} (nm)
CS1	**1**-SiNP3	butyl methacrylate	no	600 ± 30	610
CS2	**1**-SiNP6	butyl methacrylate	no	900 ± 70	840
CS3	**1**-SiNP5	methyl methacrylate	no	890 ± 40	890
CS4	**1**-SiNP5	methyl methacrylate	yes	880 ± 30	880

particle deposition on the substrate due to their size and large density. The value obtained for the hydrodynamic diameter using this technique was similar to the value calculated from the particle diameter obtained by TEM for SiNP1. The w_0 parameter for each CS sample was then calculated by calibration of the system with the corresponding silica particles used as the core in the synthesis (Table 2). The hydrodynamic diameter (D_H) values obtained for the core−shell nanoparticles are very similar to that of the expected diameter (D_{calc}), calculated from the mass balance of the synthesis procedure (Table 2). The close agreement between estimated and calculated core−shell particle diameters indicates that the amount of pure polymer particles is small. To confirm this, we have tried to separate the pure polymer material by centrifugation. These experiments showed that after centrifugation of the core−shell particles in water the supernatant is not completely transparent, but no difference could be detected in the weight of particles after careful drying of the precipitate. The centrifugation conditions (10 min at 21000rpm) were chosen so that a sample containing pure PBMA particles of 100 nm diameter in water showed no precipitation.

Hybrid core−shell nanoparticles combine the properties of the silica and the polymer components.[32] In films cast from PBMA coated silica particles, the polymer shell gives flexibility and excellent optical properties, while the silica core is expected to improve the mechanical properties of the final material as previously reported.[11] These films are cast from water dispersions of the nanoparticles at a temperature close to the T_g of the polymer in water, allowing water evaporation and deformation of the particle shells to occupy the voids between particles. In order to obtain transparent and flexible films with good mechanical properties (Figure 10), the dried films were annealed for 60 min at 90 °C to allow interdiffusion of the polymer occupying the space between the silica particles in the film. These nanohybrid films are also photoactive under an appropriate excitation wavelength. In Figure 10C we show a fluorescence image obtained from CS1 nanoparticles under 450 nm excitation (blue excitation light was filtered). The presence of fluorescence derivatives in the particle silica core opens more potential applications for the nanoparticles. With the increased dye photostability from the encapsulation in the silica particle, the core−shell hybrid particles can be used in imaging applications,[3] optical sensors,[8] or photoactive materials.[9]

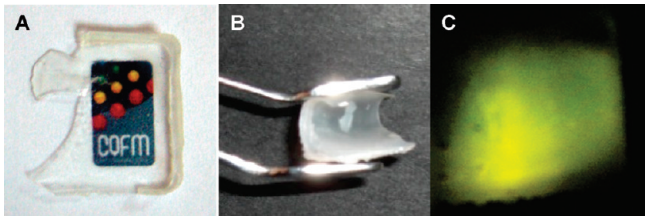

Figure 10. Images of a CS1 film obtained after 60 min of annealing at 90 °C, showing transparency (A), flexibility (B), and strong fluorescence emission under excitation at λ_{exc} = 450 nm (C).

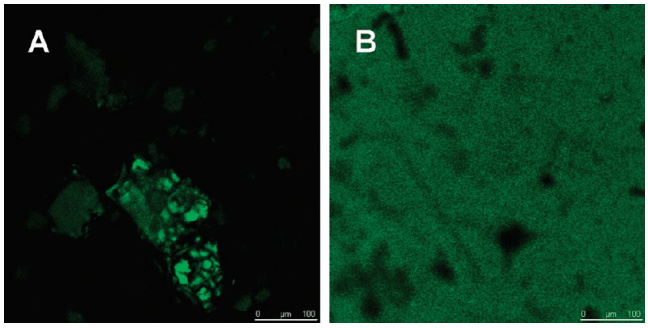

Figure 11. Laser scanning fluorescence confocal images (0.5 × 0.5 mm) of films obtained by blending water dispersions of **1**-SiNP3 with PBMA nanoparticles of 100 nm diameter using the same silica volume fraction as in the CS1 particles show aggregates of fluorescent silica particles and large dark polymer domains (A). Films cast from CS1 water dispersions show a homogeneous fluorescence distribution (B). Both films were cast from water dispersion, dried at 32 °C, and annealed at 90 °C for 1 h.

Films obtained from hybrid core−shell particles have much better properties than film obtained from mixing PBMA nanoparticles with the same content of pure silica nanoparticles. The reason for this is that in the first case the silica is homogeneously dispersed in the polymer matrix formed by the particle shells, while in the polymer/silica blend films the silica particles tend to aggregate and segregate from the material. This is observed in laser scanning fluorescence confocal microscopy (LSCFM) images of films cast from water dispersions and annealed at 90 °C for 1 h. The films obtained by blending water dispersions of **1**-SiNP3 and PBMA nanoparticles of 100 nm diameter, using the same silica volume fraction as in the CS1 particles and the same casting procedure (both films were cast from water dispersion, dried at 32 °C, and annealed at 90 °C for 1 h), show that the silica nanoparticles are segregated from large polymer domains (Figure 11A), whereas films cast from CS1 water dispersions show a homogeneous distribution of the fluorescent silica cores except for some drying defects (Figure 11B). Some degree of order is expected in films cast from water dispersions of the hybrid core−shell particles and slowly evaporated. This order can partially be observed in LSCFM images at high magnification (Supporting Information); however, the quality of these images remains a challenge because the individual particles are heavily blurred by light scattered by particles below and/or above the focus plane.

4. Conclusions

In conclusion, we were able to prepare silica nanoparticles doped with perylenediimide derivatives, by the Stöber method, with a wide range of diameters. The perylenediimide derivatives were covalently incorporated in the silica network during the synthesis, or immobilized on the surface in a postsynthesis modification procedure. The photophysical behavior of the perylenediimide derivatives on the nanoparticles is similar to that observed in toluene, with a slight degree of aggregation and fluorescence emission dependence on the environment polarity, with better photoresistance being obtained for particles labeled inside than on the surface. A polymer shell was

synthesized through emulsion polymerization, using methyl or butyl methacrylate as monomer. The diameters of the core−shell nanoparticles were characterized by fluorescence correlation spectroscopy, after calibration using the fluorescent silica core. The diameters determined with FCS are similar to the expected values from the mass balance. The fluorescent core−shell nanoparticles can be cast into strong, transparent, and flexible films. The nanoparticles developed in this work open a promising route for the production of new high performance coating materials and paints.

Acknowledgment. This work was partially supported by Fundação para a Ciência e a Tecnologia (FCT, Portugal) and POCI 2010 (FEDER) within project PDCT/CTM/68451/2006. The authors thank Dr. Aleksander Fedorov (CQFM−IN) for technical assistance with the picosecond lifetime decays and Prof. M. G. Moffitt (University of Victoria, Canada) for helpful discussions.

Supporting Information Available: FCS autocorrelation curves for the core−shell nanoparticles and LSCFM images of ordered core−shell nanoparticles in a film. This material is available free of charge via the Internet at http://pubs.acs.org.

References and Notes

(1) Astruc, D. *Nanoparticles and Catalysis*; Wiley-VCH: Weinheim, 2007.
(2) Trewyn, B. G.; Slowing, I. I.; Giri, S.; Chen, H.-T.; Lin, V. S.-Y. *Acc. Chem. Res.* **2007**, *40*, 846.
(3) Kim, J.; Piao, Y.; Hyeon, T. *Chem. Soc. Rev.* **2009**, *38*, 372.
(4) Burns, A.; Owb, H.; Wiesner, U. *Chem. Soc. Rev.* **2006**, *35*, 1028.
(5) Piao, Y.; Burns, A.; Kim, J.; Wiesner, U.; Hyeon, T. *Adv. Funct. Mater.* **2008**, *18*, 1.
(6) Yan, J.; Estévez, M. C.; Smith, J. E.; Wang, K.; He, X.; Wang, L.; Tan, W. *Nano Today* **2007**, *2*, 44.
(7) Hoffmann, F.; Cornelius, M.; Morell, J.; Froba, M. *Angew. Chem. Int. Ed.* **2006**, *45*, 3216.
(8) Borisov, S. M.; Klimant, I. *Analyst* **2008**, *133*, 1302.
(9) Klichko, Y.; Liong, M.; Choi, E.; Angelos, S.; Nel, A. E.; Stoddart, J. F.; Tamanoi, F.; Zink, J. I. *J. Am. Ceram. Soc.* **2009**, *92*, S2.
(10) Soloukhin, V. A.; Posthumus, W.; Brokken-Zijp, J. C. M.; Loos, J.; de With, G. *Polymer* **2002**, *43*, 6169.
(11) Zou, H.; Wu, S.; Shen, J. *Chem. Rev.* **2008**, *108*, 3893.
(12) Shang, X. Y.; Zhu, Z. K.; Yin, J.; Ma, X. D. *Chem. Mater.* **2002**, *14*, 71.
(13) Ray, S. S.; Okamoto, M. *Prog. Polym. Sci.* **2003**, *28*, 1539.
(14) Hong, C.-Y.; Li, X.; Pan, C.-Y. *Eur. Polym. J.* **2007**, *43*, 4114.
(15) Sugimoto, H.; Daimatsu, K.; Nakanishi, E.; Ogasawara, Y.; Yasumura, T.; Inomata, K. *Polymer* **2006**, *47*, 3754.
(16) Bauer, F.; Ernst, H.; Hirsch, D.; Naumov, S.; Pelzing, M.; Sauerland, V.; Mehnert, R. *Macromol. Chem. Phys.* **2004**, *205*, 1587.
(17) Zhang, K.; Chen, H. T.; Chen, X.; Chen, Z. M.; Cui, Z. C.; Yang, B. *Macromol. Mater. Eng.* **2003**, *288*, 380.
(18) (a) Zhang, S. W.; Zhou, S. X.; Weng, Y. M.; Wu, L. M. *Langmuir* **2005**, *21*, 2124. (b) Zhou, J.; Zhang, S. W.; Qiao, X. G.; Li, X. Q.; Wu, L. M. *J. Polym. Sci. Part A: Polym. Chem.* **2006**, *44*, 3202.
(19) (a) Bourgeat-Lami, E.; Lang, J. *J. Colloid Interface Sci.* **1998**, *197*, 293. (b) Bourgeat-Lami, E.; Lang, J. *J. Colloid Interface Sci.* **1999**, *210*, 281.
(20) Chung, P.-W.; Kumar, R.; Pruski, M.; Lin, V. S.-Y. *Adv. Funct. Mater.* **2008**, *18*, 1390.
(21) Karg, M.; Wellert, S.; Pastoriza-Santos, I.; Lapp, A.; Liz-Marzanc, L. M.; Hellweg, T. *Phys. Chem. Chem. Phys.* **2008**, *10*, 6708.
(22) Wang, H.; Peng, M.; Zheng, J.; Li, P. *J. Colloid Interface Sci.* **2008**, *326*, 151.
(23) Sondi, I.; Fedynyshyn, T. H.; Sinta, R.; Matijevic, E. *Langmuir* **2000**, *16*, 9031.
(24) Percy, M. J.; Michailidou, V.; Armes, S. P.; Perruchot, C.; Watts, J. F.; Greaves, S. J. *Langmuir* **2003**, *19*, 2072.
(25) Luo, Y.; Lin, J. *J. Colloid Interface Sci.* **2006**, *297*, 625.
(26) Pasaogullari, N.; Icil, H.; Demuth, M. *Dyes Pigm.* **2006**, *69*, 118.
(27) Stöber, W.; Fink, A.; Bohn, E. *J. Colloid Interface Sci.* **1968**, *26*, 62.
(28) Liu, X.; Zhao, H.; Li, L.; Yan, J.; Zha, L. *J. Macromol. Sci. A* **2006**, *43*, 1757.
(29) Farinha, J. P. S.; Martinho, J. M. G.; Pogliani, L. *J. Math. Chem.* **1997**, *21*, 131.
(30) (a) Moffitt, M.; Farinha, J. P. S.; Winnik, M. A.; Rohr, U.; Mullen, K. *Macromolecules* **1999**, *32*, 4895. (b) Keivanidis, P. E.; Howard, I. A.; Friend, R. H. *Adv. Funct. Mater.* **2008**, *18*, 3189.
(31) Schärtl, W. *Light Scattering from Polymer Solutions and Nanoparticle Dispersions*; Springer: Berlin, 2007.
(32) Crosby, A. J.; Lee, J.-Y. *Polym. Rev.* **2007**, *47*, 217.

JP906748R